Redox Balance and Repair Fidelity Govern the Continuum of Radiation Effects in Plants

Luis Felipe Medeiro Alves[1,2,*], **Laura Sirianni Medeiro Alves**[2], **Valter Arthur**[1,3]

[1]Institute of Energy and Nuclear Research (IPEN), University of São Paulo (USP), 05508-000 São Paulo, Brazil
[2]School of Education, Humanities and Languages (ESEHL), International University Center (UNINTER), 80020-020 Curitiba, Brazil
[3]Center for Nuclear Energy in Agriculture (CENA), University of São Paulo (USP), 13400-970 Piracicaba, Brazil

[*]Email: alves.luis@alumni.usp.br

Abstract

Ionizing radiation exerts both beneficial and deleterious effects on plants, depending on dose, rate and physiological state. Historically, two distinct research traditions have emerged: the *genetic paradigm*, focused on high-dose mutagenesis for breeding, and the *physiological paradigm*, focused on low-dose stimulation known as radiohormesis. Although often treated as independent, both derive from the same underlying radiochemical and biochemical chain of events: energy deposition, reactive oxygen species (ROS) formation, antioxidant response and repair fidelity. This paper proposes a unifying theoretical framework in which physiological, mutagenic and sterilizing outcomes appear as continuous manifestations of a single dynamic balance between ROS generation and repair throughput. A minimal kinetic model is introduced, coupling ROS accumulation, inducible antioxidant capacity and cumulative lesion load. From these relations, a dimensionless *repair challenge number* (Ξ) is derived, serving as the control parameter that orders the transition between adaptive, mutagenic and lethal regimes. Building on this kinetic foundation, we formulate an analytical dose–response model, $E(D)$, intended as a phenomenological summary of the redox–repair balance. The formulation reproduces a hormetic rise at low doses and adamage-dominated decline at higher doses. Analytical results suggest the existence of an interior maximum and, under standard unimodality assumptions, its operational uniqueness corresponding to optimal physiological response, while a fidelity function $F(D)$ links this maximum to the onset of mutational inaccuracy. Together, these relations help clarify why small variations in dose, rate or genotype can shift outcomes from stimulation to inhibition or mutation.

Keywords: Ionizing radiation, radiohormesis, repair fidelity, reactive oxygen species, mutation breeding, plant physiology, dose–response modeling

2020 MSC classification number: 92C45, 92C80, 92D10, 34C60, 92-10

1. INTRODUCTION

Ionizing radiation has occupied a relevant position in agricultural and biological sciences for more than seven decades. Initially introduced as an auxiliary tool for mutation breeding and post-harvest sterilization, its use has since expanded substantially. The same physical process that can disrupt chromosomes and generate heritable mutations can, under milder conditions, enhance germination, vigor and stress tolerance. This apparent paradox has given rise to two conceptual traditions within nuclear agronomy that, although historically separate, share a common mechanistic foundation [1].

The *Genetic paradigm* focuses on high- or moderate-dose irradiation (typically 100–400 Gy for most crops), used to induce heritable genetic variation for plant breeding. Mutation breeding programs, standardized since the mid-twentieth century under FAO/IAEA coordination, have produced more than 3,450 records of mutant varieties across more than 70 plant species in the FAO/IAEA Mutant Variety Database [4], encompassing cereals, legumes, fruits and ornamentals [9], [8].

The *Physiological paradigm* examines the non-heritable and (very) often transient effects of sublethal exposures (generally below 20 Gy, sometimes much less) on living tissues, where radiation acts as a mild stressor triggering adaptive and stimulatory responses. This biphasic pattern of enhancement at low doses and

[*]Corresponding Author
Received 10^{th} November, 2025, Revised May 4^{th}, 2026, Accepted for publication May 25^{th}, 2026. e-ISSN: 2549-2896, DOI:10.5614/cbms.2026.9.1.8

inhibition at high doses, termed *radiohormesis*, has been observed in numerous species and physiological endpoints [11], [10].

Recent studies further illustrate the species- and endpoint-dependence of plant responses to gamma irradiation. Seed and early-plant experiments in *Phaseolus vulgaris*, soybean and sesame show that irradiation outcomes vary with species, dose, developmental stage and target trait, supporting the need for a parameterized rather than universal threshold model [5], [7], [6].

Although these paradigms developed independently (one emphasizing genetic innovation and the other physiological regulation) both originate from the same fundamental chain of interactions between ionizing energy and biological matter. In every case, the initial event is the ionization of water molecules and organic compounds, producing reactive oxygen species (ROS) such as hydroxyl radicals ($OH\cdot$), superoxide ($O_2^{\cdot -}$) and hydrogen peroxide (H_2O_2). These species act simultaneously as agents of damage and as signaling intermediates. Whether the outcome manifests as stimulation, mutation or lethality depends on the dynamic balance between ROS generation, detoxification and repair fidelity, a balance modulated by dose, dose rate, tissue hydration and genetic background.

Historically, radiation physiology and mutation breeding were treated as separate disciplines. Mutation breeders exposed dry seeds to hundreds of gray, seeking permanent DNA alterations, but physiologists irradiated hydrated seeds with a few gray, seeking transient metabolic activation. Yet recent experimental and theoretical advances increasingly reveal these as contiguous segments of a single dose–response continuum rather than categorically different processes.

At low doses, ROS transients activate redox-sensitive transcription factors, mitogen-activated protein kinase (MAPK) cascades and hormonal crosstalk involving auxins, cytokinins, and abscisic acid. These responses enhance reserve mobilization, accelerate germination and strengthen antioxidant defenses [3]. At higher doses, the same radical species accumulate beyond repair capacity, producing irreversible DNA lesions, chromosomal aberrations and cell death. Between these extremes lies a narrow regime where repair remains efficient but error-prone, giving rise to stable mutations without catastrophic failure. Thus, hormesis, mutagenesis and sterilization can be understood not as discrete categories but as overlapping domains governed by the same biochemical kinetics under different parameter ranges.

Classical studies by [11] already recognized that the biological effect of radiation depends not only upon the total energy absorbed but upon the physical conditions of exposure and the physiological condition of the material irradiated. Later work confirmed that minor variations in seed moisture, oxygen tension or dose rate can shift a treatment from stimulatory to inhibitory, demonstrating that the boundaries between regimes are fluid rather than fixed [9].

The dual character of radiation (destructive at high intensity yet stimulatory at low intensity) has been recognized since the early decades of nuclear agronomy. In the 1950s and 1960s, international programs under the FAO and IAEA formalized the use of ^{60}Co and ^{137}Cs irradiators for both seed treatment and pest control. Their standardized protocols defined absorbed dose (D, in gray), dose rate and seed moisture as the primary experimental variables. The same guidelines that ensured reproducibility in mutation breeding now provide the methodological foundation for studying low-dose effects.

During this institutionalization, the conceptual divergence between "beneficial" and "harmful" effects reflected not a physical dichotomy but a limitation of the available theoretical framework. Without a unified kinetic model, radiation biologists classified outcomes empirically: sublethal stimulation was labeled physiological, lethal or mutagenic effects were labeled genetic. Yet as [11] anticipated, these outcomes differ only in degree and timescale. The same cascade of radiolytic reactions (ionization, radical formation, oxidative signaling and repair) underlies all radiation responses. What varies is the proportion of energy channeled into adaptive signaling versus irreversible damage.

At the molecular level, the link between the physiological and genetic regimes is the interplay between oxidative signaling and repair fidelity. Ionizing radiation initiates water radiolysis:

$$H_2O \xrightarrow{\text{radiation}} H\cdot,\ OH\cdot,\ e^-_{aq},\ H_2O_2,\ H_2.$$

The transient ROS burst modifies redox potential and triggers both antioxidant and DNA-repair pathways. When ROS remain within the dynamic range that cellular detoxification can handle, the system exhibits adaptive activation: antioxidant enzymes (superoxide dismutase, catalase, peroxidases) increase, reserve mobilization accelerates and growth is enhanced. When ROS exceed this range, oxidative lesions accumulate faster than repair, leading to mutations or catastrophic outcomes.

This duality can be summarized by the ratio between effective ROS load (R) and cellular repair capacity (R_c):

$$R < R_c \Rightarrow \text{adaptive stimulation (hormesis)}, \tag{1}$$

$$R \approx R_c \Rightarrow \text{mutation threshold}, \tag{2}$$

$$R \gg R_c \Rightarrow \text{cellular collapse}. \tag{3}$$

The transition among these regimes is continuous and reflects the same underlying kinetics. Recent modeling efforts have begun to formalize this principle mathematically, introducing parameters that capture the balance between radical generation and repair throughput.

The empirical regularity of biphasic dose–response curves across taxa suggests that some kind of universal mathematical structure governs radiation–plant interactions. Phenomenological models such as the Brain–Cousens equation have long captured hormetic responses:

$$E(D) = c + \frac{(d-c) + fD}{1 + (D/e)^b},$$

where $E(D)$ represents a biological endpoint (growth, germination or yield) as a function of dose D. While effective descriptively, such equations remain empirically fitted and lack mechanistic grounding. The present work aims to suggest a unified dose–effect model from explicit redox–repair dynamics. In this framework, the hormetic term arises naturally from the activation of signaling pathways, while the decline at high doses reflects the accumulation of unrepaired lesions.

The necessity for a rigorous synthesis is both conceptual and practical. Conceptually, it clarifies that physiological hormesis and genetic mutation are not qualitatively different but quantitatively distinct manifestations of the same process. Practically, it enables predictive modeling of dose windows that optimize stimulation without incurring mutagenic risk. Such predictive capacity is essential for reproducibility and for integrating radiation treatments into precision agriculture, where small dose deviations can shift outcomes dramatically [1].

The objective of this paper is therefore to construct a quasi-framework unifying the physiological and genetic paradigms of radiation effects in plants. We aim to show that both are limiting cases of a continuous process governed by redox kinetics and repair dynamics. Specifically, we will:

1) Derive a minimal kinetic model linking ROS generation, antioxidant activation and lesion repair, from which a single control parameter (the *repair challenge number* (Ξ)) can be seen as the determinant of regime boundaries.
2) Formulate a unified dose–effect model $E(D)$ that analytically reduces to the Brain–Cousens hormetic curve at low doses and to the classical monotonic damage model at high doses.
3) Demonstrate, under mild mathematical conditions, the existence and uniqueness of an interior maximum (the hormetic peak) and the continuity of the transition toward mutagenic and sterilizing regimes.

The framework does not propose new empirical findings, it rather integrates decades of observations under a single quantitative language. Its aim is to provide a common theoretical substrate on which both physiological stimulation and mutation breeding can be understood as expressions of the same radiobiological continuum.

Recognizing this continuum has practical and philosophical implications. It situates radiation within the general class of stress–response phenomena governed by nonlinear feedback between damage and repair, aligning plant radiobiology with other domains of adaptive toxicology. It also reconciles two traditions of nuclear agronomy (the physiological and the genetic) that have long progressed in parallel.

2. METHODOLOGY

Ionizing radiation interacts with plant tissues through a series of well-defined physical and chemical steps that ultimately converge on a limited number of biological outcomes. Whether a given exposure leads to stimulation, mutation or lethality depends not on the qualitative nature of the agent (which is the same in all cases) but on quantitative differences in the intensity, duration and spatial distribution of reactive intermediates. This section develops a mechanistic interpretation of these processes and introduces the formal parameters that govern their transitions.

No new irradiation experiment was performed in this study. Consequently, no single plant material, organ, genus or species was irradiated by the authors. The framework is formulated for plant tissues in general, while seed irradiation is used as the principal reference case because most low-dose radio-stimulation and mutation-breeding protocols are reported for seeds and early seedlings. Species, organ type, hydration state and developmental stage are therefore treated as biological modifiers of the model parameters, rather than as fixed experimental inputs.

The initial interaction between ionizing radiation and biological matter is primarily physical. When gamma or X rays traverse hydrated tissues, they deposit energy that ionizes water molecules and, to a lesser extent, organic constituents. The immediate result is the formation of primary radicals, such as hydroxyl (OH·), hydrated electrons (e^-_{aq}) and hydrogen atoms (H·). These highly reactive species initiate a cascade of secondary chemical reactions collectively known as water radiolysis. Within microseconds, the system reaches a quasi–steady-state composition dominated by reactive oxygen species (ROS) such as hydrogen peroxide (H_2O_2) and superoxide ($O_2^{\cdot -}$). These intermediates diffuse through the cytoplasm, interacting with proteins, membranes, nucleic acids and organellar components.

This universal chain of events can be summarized as follows: (i) Energy deposition: Radiation transfers discrete quanta of energy to water and biomolecules, initiating ionization and excitation events. (ii) Primary radical generation: Each ionization event yields short-lived radicals (OH·, e^-_{aq}, H·). (iii) Secondary chemistry: Radical recombination and disproportionation generate longer-lived ROS (H_2O_2, $O_2^{\cdot -}$). (iv) Cellular response: ROS interact with macromolecules, activating signaling cascades or producing molecular damage depending on concentration and duration.

Although simple in outline, this sequence embodies the dual character of radiation action: the same species that mediate physiological stimulation at low concentrations cause cytotoxicity when accumulated beyond the capacity of antioxidant systems. From a mechanistic perspective, the difference between beneficial and deleterious outcomes is not in the identity of the radicals but in their steady-state levels and spatial confinement.

Let $R(t)$ denote the instantaneous intracellular concentration of ROS and $A(t)$ the effective antioxidant capacity. To a first approximation, the kinetics of ROS accumulation can be described by a balance equation,

$$\frac{dR}{dt} = \kappa u(t) - \sigma_R R - \eta R^2,$$

where $u(t)$ is the dose rate (in $\mathrm{Gy\,h^{-1}}$), κ converts physical dose rate to radical generation rate, σ_R represents linear scavenging and ηR^2 captures nonlinear recombination. At low R, the quadratic term can be neglected, leading to a steady-state level $R^* \approx \kappa u/\sigma_R$. This relationship formalizes the intuitive idea that ROS concentration increases proportionally with dose rate until other processes (antioxidant consumption, diffusion or recombination) intervene.

The antioxidant response can be modeled as a feedback system:

$$\frac{dA}{dt} = \alpha_0 + \alpha_1 R - \sigma_A A,$$

with α_0 representing basal synthesis, $\alpha_1 R$ inducible synthesis, and σ_A degradation. These coupled equations encapsulate the self-limiting nature of oxidative stress: radiation raises ROS, ROS induces antioxidants and antioxidants in turn limit ROS accumulation. Depending on parameters, the system can exhibit three qualitative regimes corresponding to stimulation, adaptation and breakdown. This dynamic constitutes the biochemical substrate of radiohormesis.

Within this kinetic framework, the biological outcome of irradiation can be characterized by the ratio of two competing fluxes: the rate of radical generation and the rate of damage repair or detoxification. We define the instantaneous ROS load R as proportional to the absorbed dose rate and the effective repair capacity R_c as a composite measure of enzymatic and nonenzymatic defenses. The relative magnitude of these two quantities defines three distinct regimes, as defined above. Each regime represents a dynamic equilibrium rather than a fixed boundary. Small shifts in dose rate, hydration or genotype can move the system from one to another. Briefly, here are the characteristics of each:

Hormesis: When the ROS burden remains below repair capacity, the system responds adaptively. Transient oxidation of redox-sensitive proteins activates signaling pathways such as MAPK cascades and transcription factors controlling antioxidant enzymes. DNA repair systems are upregulated and cellular metabolism accelerates. In this regime, repair is assumed to be essentially error-free and the net effect is improved

physiological performance: faster germination, greater vigor and increased tolerance to subsequent stress. Mathematically, this corresponds to a stable steady state of the ROS–antioxidant system with $R^* < R_c$ and negative feedback dominating.

Table 1: Continuum of radiation effects in plants as governed by the repair challenge number (Ξ). The same redox–repair dynamics produce distinct biological outcomes under different parameter ranges.

Regime	Dominant condition	Characteristic response	Typical experimental range (seeds)
Hormetic / Adaptive	$\Xi \ll 1$; $R < R_c$; $F(D) \approx 1$	Transient ROS signaling; enhanced antioxidant activity; stimulation of germination, vigor and stress tolerance	0.1–30 Gy (strongly species-dependent)
Mutagenic / Transitional	$\Xi \approx 1$; $R \simeq R_c$; $F(D) \downarrow$	Repair becomes partially error-prone; stable mutations without catastrophic loss of function	50–600 Gy (typical range for mutation breeding)
Sterilizing / Lethal	$\Xi \gg 1$; $R \gg R_c$; $F(D) \to 0$	Repair collapse, loss of viability, chromosomal fragmentation, membrane breakdown	$>$ 1000 Gy (depending on tissue and hydration)

Mutation: As dose increases and R approaches R_c, repair becomes partially error-prone. The antioxidant and DNA repair systems operate near saturation and stochastic errors in lesion processing appear. A fraction of double-strand breaks are misrepaired, leading to small insertions, deletions, or chromosomal rearrangements. This intermediate regime bridges physiological adaptation and genetic alteration. It is the operational domain of mutation breeding. The transition is not abrupt but gradual: the probability of misrepair rises smoothly with R/R_c. In kinetic terms, the system approaches a critical point where feedback delays and finite repair speed induce fluctuations around the steady state.

Sterilization: Beyond this threshold, ROS accumulation overwhelms all compensatory mechanisms. Antioxidant pools are depleted, repair enzymes become inactivated and cell membranes undergo lipid peroxidation. The system loses stability, leading to irreversible structural damage and death. In seeds or meristematic tissues, this corresponds to loss of viability or failure of division. In the minimal equations, this regime should not be interpreted as a literal divergence of R^* for finite u. Rather, it corresponds to a situation in which the steady oxidative and lesion burden exceeds the effective repair margin, so that viability or reproductive function collapses even though the coarse-grained variables remain mathematically finite. This catastrophic transition defines the sterilization threshold used in phytosanitary irradiation.

Although described as distinct, these regimes form a continuous spectrum governed by the same underlying equations. The boundaries $R \approx R_c$ and $R \gg R_c$ are operational constructs that depend on the *definition* of failure or viability. Empirically, reported ranges span roughly a few gray (hormesis), hundreds of gray (mutation), and thousands of gray (sterilization), but they vary widely by species, tissue, hydration and oxygenation.

Graphically, this continuum can be represented by a composite curve of biological performance $E(D)$ versus absorbed dose D (Figure 1). The curve rises at low doses as signaling dominates, reaches a maximum near $R = R_c$, and declines as damage accumulates. The horizontal axis thus represents increasing energy input, while the vertical axis represents net functional output (germination, growth or survival). Annotating the curve with dominant processes (signaling/hormesis, mutation, lethality/sterilization) emphasizes that no discontinuity exists between physiological and genetic domains.

While the ratio R/R_c captures the instantaneous balance between stress induction and defensive capacity, the long-term outcome depends on the fidelity of damage repair. We introduce a function $F(D)$ representing the fraction of DNA lesions repaired faithfully after a cumulative absorbed dose D, which decreases sigmoidally beyond a characteristic dose D_f:

$$F(D) = \frac{1}{1 + (D/D_f)^p}.$$

Here, D_f denotes the dose at which repair fidelity declines to half its baseline value, and $p > 0$ controls the steepness of this transition. The complement $1 - F(D)$ quantifies the fraction of lesions that are misrepaired or remain unrepaired.

This sigmoidal expression is phenomenological. It is not intended to specify a particular molecular repair pathway, but to summarize the empirically plausible loss of repair accuracy as accumulated dose and repair demand increase.

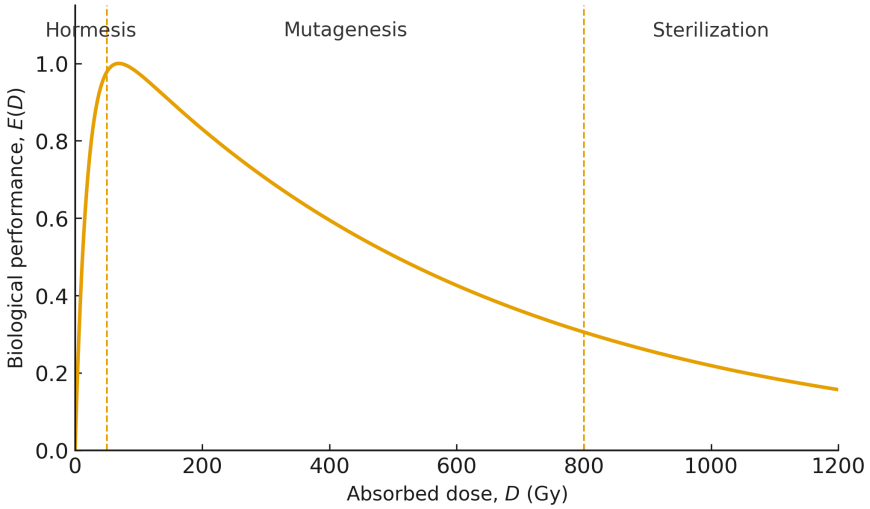

Figure 1: Composite curve of biological performance $E(D)$ as a function of absorbed dose D. The curve illustrates three overlapping domains: hormetic stimulation, mutagenic instability and sterilization. The curve is schematic and is not fitted to a specific dataset. Its purpose is to illustrate the proposed ordering of regimes along the dose axis, not to assign universal threshold values.

The expected mutagenic load, proportional to the product of total lesion burden and repair inaccuracy, is therefore

$$M(D) = R^*(u)\,[1 - F(D)], \quad u \equiv D/T \text{ (constant-rate exposure).}$$

We make explicit the bridge between repair fidelity and the challenge index. Assume a monotone map $\hat{F}$ such that $F(D) = \hat{F}(\Xi(D))$ with $\hat{F}(\Xi) \approx \left[1 + (\Xi/\Xi_f)^{\tilde{p}}\right]^{-1}$. Under constant-rate exposure, $\Xi = \Xi(u)$ and $u = D/T$, hence the characteristic dose D_f satisfies $\Xi(u_f) = \Xi_f$ with $u_f = D_f/T$. This identifies D_f with the onset of $\Xi \approx 1$ (repair saturation) and makes the F–Ξ connection explicit.

This formulation links physiological and genetic responses within a single parameterization. At low doses ($D \ll D_f$), $F(D) \approx 1$, implying high-fidelity repair and negligible mutation. In this regime, ROS act as signaling molecules and the biological response is stimulatory. As D approaches D_f, $F(D)$ declines, introducing a nonzero probability of misrepair, entering the mutagenic regime. At very high doses ($D \gg D_f$), $F(D)$ tends toward zero and repair collapses, leading to sterilization.

The parameters D_f and p are species- and genotype-dependent. Varieties with strong antioxidant systems or efficient DNA repair exhibit higher D_f (they tolerate greater doses before fidelity declines) and often smaller p (a more gradual transition). Conversely, radiosensitive genotypes have lower D_f and steeper p, implying abrupt loss of repair accuracy. These parameters therefore encapsulate radiosensitivity in a mathematically concise form.

The function $F(D)$ also provides a direct link to empirical observations. In mutation breeding, the semi-lethal dose (LD_{50}) often correlates with the dose where $F(D) \approx 0.5$, as a heuristic proxy. In physiological studies, the dose of maximal stimulation corresponds to the maximum of $E(D)$, defined by the condition $\frac{dE}{dD} = 0$. As analyzed below, these two conditions are related through the dependence of $E(D)$ on both $F(D)$ and $R^*(u)$. Consequently, the same mathematical entity, repair fidelity, governs both the hormetic peak and the onset of mutagenesis.

The characteristic dose D_f can be viewed as a quantitative expression of biological resilience. It aggregates multiple molecular processes: the efficiency of radical scavenging, the speed of enzymatic repair and the structural stability of macromolecules. The exponent p reflects the cooperativity or threshold behavior of repair failure; high values of p produce sharp transitions between regimes, while low values yield gradual declines. These abstractions do not replace molecular detail but offer a compact phenomenological link

between measurable doses and biological outcomes.

Genetic and environmental factors modulate D_f and p. Species adapted to high oxidative environments, such as halophytes, would exhibit large D_f values, consistent with broad hormetic windows. Pre-conditioning or seed priming with mild stress can temporarily increase D_f, a phenomenon known as adaptive response. Conversely, nutrient deficiency, aging or hypoxia are expected to reduce D_f, narrowing the tolerance range. In breeding or biotechnology contexts, these parameters could serve as quantitative targets: enhancing repair fidelity or antioxidant capacity effectively shifts the hormetic window to higher doses, expanding the useful range of radiation treatments.

The passage from the dynamical variables $R(t)$, $A(t)$ and $X(t)$ to a scalar endpoint $E(D)$ is a change of observational scale. The ordinary differential equations describe the time evolution of aggregated biochemical state variables, whereas $E(D)$ summarizes a macroscopic endpoint measured after exposure, such as germination, early biomass, vigor or survival. Thus, $E(D)$ is not claimed to be an exact closed-form solution of Eqs. (4)–(6); it is a phenomenological dose–response formulation whose parameters can be interpreted through the repair challenge index Ξ.

Combining these elements yields a coherent description of radiation–plant interaction across all scales. Under a specified irradiation protocol $u(t)$, the average ROS load is $R^*(u)$; for constant-rate exposures $u = D/T$. The ratio R^*/R_c marks immediate physiological regimes and the function $F(D)$ determines the long-term fidelity of recovery. The overall biological effect can then be expressed as a balance between stimulation and damage,

$$E(D) = S_0 + S(R(D)) - L(M(D)),$$

where $S(R)$ is an increasing, saturating function representing beneficial signaling and $L(M)$ an increasing function representing cumulative loss due to mutagenic or lethal events. In subsequent sections, this conceptual relation will be formalized into an explicit analytical model $E(D)$ that spans hormesis, mutation and sterilization.

This framework is deliberately minimalistic. It does not invoke new biochemical species or speculative pathways but reorganizes established knowledge into quantitative form. With a small set of parameters (dose D, ROS load R, repair capacity R_c and fidelity $F(D)$) it could capture the essence of diverse experimental results. Moreover, it offers testable predictions: (i) the position of the hormetic maximum should correlate with D_f, (ii) varieties with higher R_c should exhibit both delayed onset of inhibition and reduced mutation frequency, and (iii) adaptive pretreatments that increase antioxidant capacity should shift the entire dose–response curve rightward without altering its shape.

In what follows we develop an economical kinetic scheme that (i) adheres to standard radiochemical and physiological knowledge, (ii) yields a transparent *single* nondimensional control parameter separating regimes, and (iii) connects cleanly to measurable dose–response observables used in seed physiology and mutation breeding. The goal here is to provide a mathematically explicit scaffold that organizes existing phenomena, rather than propose mechanistic novelties.

We adopt three lumped state variables: the transient reactive oxygen species pool $R(t)$ (arbitrary concentration units), an inducible antioxidant capacity $A(t)$ (arbitrary activity units) and a cumulative DNA lesion load $X(t)$ (double-strand-break equivalents or another consistent lesion proxy). Radiation is delivered with dose-rate $u(t)$ (Gy·time^{-1}). The minimal dynamical system is

$$\dot{R} = \kappa\, u(t) - \sigma_R R - \eta R^2, \tag{4}$$

$$\dot{A} = \alpha_0 + \alpha_1 R - \sigma_A A, \tag{5}$$

$$\dot{X} = \lambda R - \rho A\, X - \mu X. \tag{6}$$

All parameters are nonnegative. The terms have the following interpretations: κ converts physical dose-rate to primary/secondary radical production, σ_R models first-order (pseudo-first) scavenging and dilution, ηR^2 aggregates radical–radical termination, α_0 is basal synthesis of antioxidant machinery, $\alpha_1 R$ is inducible synthesis proportional to the oxidative signal, σ_A is antioxidant turnover/inactivation, λR is effective influx of potentially mutagenic lesions (per unit R), $\rho A\, X$ is repair throughput proportional to capacity A and current burden X and μX includes A-independent resolution (e.g. excision and other baseline processes).

We stress that (4)–(6) are *lumped* (coarse-grained) balances designed for analytical clarity. They do not attempt spatial or pathway-specific detail; rather, their value is to expose control structure and regime transitions under minimal assumptions.

We consider piecewise-constant irradiation protocols $u(t) \equiv u$ defined over exposure intervals long compared to radical lifetimes (microseconds–seconds) but short compared to organismal endpoints (hours–days). Under this standard scale separation, the fast variables R (reactive oxygen species) and A (antioxidant capacity) relax rapidly to quasi–steady states relative to the slow variable X (damage marker) and to macroscopic outcomes.

We assume throughout that all rate constants are positive:

$$\kappa,\ \sigma_R,\ \eta,\ \sigma_A > 0, \quad \text{and} \quad u \geq 0,$$

and that production terms satisfy $\alpha_0, \alpha_1 \geq 0$ so that $R(t), A(t) \geq 0$ for all admissible initial conditions.

Under constant u, the ROS balance

$$\dot{R} = \kappa u - \sigma_R R - \eta R^2.$$

is a Riccati equation with a unique nonnegative equilibrium

$$R^*(u) = \frac{-\sigma_R + \sqrt{\sigma_R^2 + 4\eta\kappa u}}{2\eta}, \qquad R^*(u) \to \frac{\kappa}{\sigma_R} u \text{ as } \eta \to 0. \tag{7}$$

The equilibrium $R^*(u)$ is globally asymptotically stable on $[0, \infty)$ since $f(R) = \kappa u - \sigma_R R - \eta R^2$ satisfies $f'(R) = -\sigma_R - 2\eta R < 0$ for all $R \geq 0$. Hence, for any $R(0) \geq 0$, the trajectory $R(t)$ converges *monotonically* to $R^*(u)$: if $R(0) < R^*(u)$ then $\dot{R} > 0$ until equilibrium, and if $R(0) > R^*(u)$ then $\dot{R} < 0$ until equilibrium.

Differentiating (7) yields the parametric sensitivities

$$\frac{\partial R^*}{\partial u} = \frac{\kappa}{\sqrt{\sigma_R^2 + 4\eta\kappa u}}, \qquad \frac{\partial^2 R^*}{\partial u^2} = -\frac{2\eta\kappa^2}{\left(\sigma_R^2 + 4\eta\kappa u\right)^{3/2}} \leq 0,$$

so that $R^*(u)$ is strictly increasing and concave in u, and the sensitivity $\partial R^*/\partial u$ decreases with u whenever $\eta > 0$.

Given $R(t)$, the antioxidant balance reads

$$\dot{A} = \alpha_0 + \alpha_1 R(t) - \sigma_A A.$$

If u is constant and $R(t)$ has relaxed to $R^*(u)$, then $A(t)$ evolves linearly toward

$$A^*(u) = \frac{\alpha_0 + \alpha_1 R^*(u)}{\sigma_A}, \tag{8}$$

with exponential convergence rate σ_A:

$$A(t) = A^*(u) + \big(A(0) - A^*(u)\big)e^{-\sigma_A t}.$$

Thus, for exposure intervals satisfying

$$T_{\text{seg}} \gg \max\left\{ (\sigma_R + 2\eta R^*)^{-1},\ \sigma_A^{-1} \right\},$$

and for slow variables X evolving on timescales $\gg T_{\text{seg}}$, the pair (R, A) may be approximated by their steady values $(R^*(u), A^*(u))$ while X integrates the net lesion flux.

Under these positivity and scale-separation conditions, (4)–(6) admit a well-defined quasi–steady-state reduction in which R and A instantaneously follow the control u via (7)–(8), and X accumulates damage at the effective steady rate implied by these balances. This approximation preserves the system's control structure and stability while allowing analytical exploration of regime transitions with minimal complexity.

We now define a compact measure of the instantaneous challenge to repair:

$$\Xi(u) \ := \ \frac{\text{inflow of potentially mutagenic lesions}}{\text{effective repair throughput}} \ = \ \frac{\lambda\, R^*(u)}{\rho\, A^*(u) + \mu}. \tag{9}$$

Since R^* increases and A^* is affine in R^*, Ξ is an increasing function of the physical drive u (and hence of dose D under fixed-rate exposures). By construction:

$$\begin{aligned}
\Xi \ll 1 &\Rightarrow \text{ adaptive regime (repair comfortably in excess),} \\
\Xi \approx 1 &\Rightarrow \text{ onset of infidelity / mutational regime,} \\
\Xi \gg 1 &\Rightarrow \text{ repair collapse / sterilizing regime.}
\end{aligned}$$

It is worth noting that Ξ is not a new physical effect but a bookkeeping of known balances: numerator from radical-driven lesion formation, denominator from A-dependent and baseline repair. It will serve as the regime index in subsequent results.

Lemma 2.1. *Monotonicity and bounds for Ξ:*
Let $u \mapsto R^*(u)$ be the positive steady state of (4), and $A^*(u) = (\alpha_0 + \alpha_1 R^*)/\sigma_A$. Then $u \mapsto \Xi(u)$ defined in (9) is continuous, strictly increasing for $u > 0$, satisfies $\Xi(0) = 0$, and has finite asymptote

$$\Xi_\infty = \lim_{u\to\infty} \Xi(u) = \frac{\lambda\,\sigma_A}{\rho\,\alpha_1} \quad \text{if } \alpha_1 > 0,$$

while $\Xi(u) \to \infty$ as $u \to \infty$ if $\alpha_1 = 0$.

If inducible antioxidants are present ($\alpha_1 > 0$), Ξ saturates: induction prevents unbounded challenge growth. If inducibility is absent or impaired ($\alpha_1 \approx 0$), Ξ can grow arbitrarily, consistent with catastrophic failure.

Under quasi-steady (R^*, A^*), the lesion balance (6) reduces to

$$\dot{X} = \lambda R^* - (\rho A^* + \mu)X \;=\; (\rho A^* + \mu)\,\big(\Xi - X\big).$$

Thus $X(t) \to X^*(u) = \Xi(u)$ exponentially with rate $\rho A^* + \mu$. In steady conditions the dimensionless challenge Ξ coincides with the normalized lesion burden. This identity provides a direct physical meaning to Ξ and will be used in stochastic arguments below.

Some immediate comparative statics of Ξ are useful for interpretation:

- $\partial\Xi/\partial\kappa > 0$: more efficient radical generation increases challenge.
- $\partial\Xi/\partial\sigma_R < 0$ and $\partial\Xi/\partial\eta < 0$: stronger ROS sinks reduce challenge.
- $\partial\Xi/\partial\alpha_1 < 0$ and $\partial\Xi/\partial\sigma_A > 0$: faster inducible antioxidant response (large α_1) lowers challenge; faster turnover (large σ_A) raises it.
- $\partial\Xi/\partial\rho < 0$ and $\partial\Xi/\partial\mu < 0$: stronger repair throughput reduces challenge.

These signs formalize common physiological intuitions (e.g., priming that raises α_1 or ρ widens the safe window).

Macroscopic endpoints (germination rate, vigor, early biomass) reflect two opposing channels: a short-term *adaptive* or *performance* channel that increases with modest oxidative signaling, and a *damage* channel accumulating with lesion misrepair. We model the net observable effect $E(D)$ at cumulative dose D as

$$E(D) = \underbrace{c + \frac{(d-c) + fD}{1 + (D/e)^b}}_{\mathcal{H}(D)\ \text{(adaptive)}} \;-\; \underbrace{q\,D^r}_{\mathcal{L}(D)\ \text{(cumulative damage)}}, \tag{10}$$

with parameters $c < d$, $f > 0$, $e > 0$, $b > 1$, $q > 0$, $r > 1$. The first term is a Brain–Cousens-like rise with an interior peak (the fD numerator captures a low-dose slope), and the second term aggregates a late penalty. This parsimonious superposition suffices to span hormesis $\to$ damage-dominated decline. We emphasize that (10) is *phenomenological* but admits a kinetic mapping through Ξ. The borderline case $r = 1$ can be treated separately; then the initial slope is $E'(0) = f - q$, so an initial hormetic rise requires $f > q$. For clarity, the main analysis below assumes $r > 1$.

In this notation, f represents the low-dose adaptive gain, and is associated with the initial sensitivity of the endpoint to ROS-mediated signaling. The scale parameter e marks the dose range in which the repair challenge approaches $\Xi \approx 1$, and therefore approximates the transition from comfortably compensated oxidative signaling to repair saturation. The exponent b controls the steepness with which the adaptive component saturates or declines, whereas q and r summarize the magnitude and dose-dependence of the accumulated damage channel. These parameters are therefore endpoint-dependent: germination, root elongation, early biomass and survival need not share identical fitted values.

Low-dose slope $f \propto \beta\,\partial R^*/\partial D$ (gain of the adaptive channel), "half-activation" e is the dose where $\Xi \approx 1$ (onset of challenge), b reflects steepness of the Ξ transition (linked to α_1, ρ, σ_A) and r summarizes how cumulative lesions depress function (linear to supra-linear depending on endpoint).

Basic shape properties of E: If $f > 0$, $b > 1$, $q > 0$, $r > 1$, then $dE/dD\big|_0 = f > 0$ and $\lim_{D\to\infty} dE/dD = -\infty$. Hence E has at least one interior maximizer $D^* > 0$. If $\mathcal{H}$ is unimodal and $\mathcal{L}$ is convex, then E is unimodal and D^* is unique.

As $q \to 0$, $E \to \mathcal{H}$ (pure hormetic form). As q increases (or r increases), the peak shifts left and shrinks, beyond a critical q the interior maximum vanishes, recovering a monotone-decreasing curve. Thus (10) continuously spans hormesis $\to$ mutation $\to$ sterilization.

Let $D_e := e$ and $E_s := d - c$ be characteristic dose and effect scales. Define nondimensional $x = D/D_e$ and $\tilde{E} = (E - c)/E_s$. Then

$$\tilde{E}(x) = \frac{1 + \phi x}{1 + x^b} - \tilde{q}\, x^r, \qquad \phi := \frac{f e}{E_s}, \qquad \tilde{q} := \frac{q\, e^r}{E_s}.$$

All qualitative shapes are governed by the triple $(\phi, b, \tilde{q})$ and the exponent r. This reduction is helpful for identifiability discussions and for comparing endpoints or varieties on a common scale.

Let x^* maximize $\tilde{E}$. For any $b > 1$, $r > 1$,

$$x^* \in \left(0,\ (\phi/\tilde{q}r)^{1/r}\right) \quad \text{and} \quad x^* \to \phi^{1/b} \quad \text{as } \tilde{q} \downarrow 0.$$

The peak dose scales approximately as $(\phi/\tilde{q})^{1/r}$ when damage is appreciable, reducing $\tilde{q}$ (e.g., via stronger repair or lower λ) or increasing low-dose gain ϕ (e.g., stronger adaptive response) both move D^* rightwards, enlarging the useful window.

The lesion variable X aggregates potential precursors of mutation. We now formalize the link from deterministic kinetics to probabilistic mutation yields. The presentation is intentionally conservative, our aim is to derive standard expressions from explicit hypotheses.

Let $N(D)$ denote the random number of *potentially mutagenic* lesion events accumulated by dose D. Under the usual sparse-event approximation and conditional independence given (R^*, A^*), a Poisson model is natural:

$$N(D) \sim \text{Poisson}\big(\Lambda(D)\big), \quad \Lambda(D) = \int_0^{T(D)} \lambda_{\text{eff}}\big(\Xi(u(t))\big)\, dt,$$

where $T(D)$ is the exposure time to reach dose D and λ_{eff} is an increasing function of challenge (more on λ_{eff} below). The probability of at least one mutational event in a target region is then

$$P_{\text{mut}}(D) = 1 - \exp\{-\Lambda(D)\}. \tag{11}$$

For constant u and quasi-steady (R^*, A^*),

$$\Lambda(D) = \frac{D}{u}\, \lambda_{\text{eff}}(\Xi(u)).$$

A common simplification is to express λ_{eff} as a dose-modulated base rate via a fidelity factor $F(D)$:

$$\lambda_{\text{eff}}(\Xi) \approx \lambda\, [1 - F(D)], \qquad F(D) = \frac{1}{1 + (D/D_f)^p}, \tag{12}$$

with λ a lesion-per-gray scale factor. Substitution into (11) recovers the convenient closed form

$$P_{\text{mut}}(D) = 1 - \exp\{-\lambda\, D\, [1 - F(D)]\}. \tag{13}$$

Equation (13) is the standard exponential no-hit expression with an effective cross-section inflated by misrepair probability $1 - F(D)$. It explicitly couples kinetic challenge (via D_f, p that encode repair infidelity onset) to mutation probability.

Because $F(D)$ declines when Ξ approaches unity (onset of saturation), the parameter D_f can be interpreted as the dose where $\Xi(D_f) \approx 1$. Thus D_f also approximates the position where the adaptive peak ceases to advance.

For small D (i.e., $D \ll D_f$), $F(D) = 1 - (D/D_f)^p + O(D^{2p})$ and

$$\Lambda(D) = \lambda\, D\, [1 - F(D)] = \lambda\, \frac{D^{p+1}}{D_f^p} + O(D^{2p+1}), \quad P_{\text{mut}}(D) = \Lambda(D) + O(\Lambda^2).$$

Hence mutation probability scales as D^{p+1} at low doses (super-linear for $p > 0$), consistent with the empirical difficulty of detecting mutagenesis in the hormetic region.

Let $D = \int_0^T u(t)\,dt$ be fixed. Because $\Xi = \Xi(u)$ is increasing and (12) is decreasing in Ξ through D_f (heuristically), protocols with higher instantaneous u produce larger $[1 - F(D)]$ for the same cumulative D, therefore larger $\Lambda(D)$ and $P_{\mathrm{mut}}(D)$. This recovers the standard dose-rate sparing: *lower dose-rates are less mutagenic at fixed dose* in as much as inducible A can develop ($\alpha_1 > 0$).

The net endpoint $E(D)$ in (10) depends on the *expected* lesion penalty, whereas P_{mut} captures the tail probability of at least one mutational event. Although distinct, both are driven by the same fidelity decline. Accordingly, we expect a positive correlation between the dose at maximal $E(D)$ and the dose at which P_{mut} becomes appreciable (both moving with D_f and with repair strength). This offers a practical cross-check: experiments reporting a right-shift of the hormetic window after priming should also observe reduced mutational yield at a fixed D.

The deterministic–stochastic synthesis above presumes scale separation typical in radiobiology:

1) *Microseconds–seconds:* energy deposition and water radiolysis drive R to R^*.
2) *Minutes–hours:* inducible antioxidant capacity A approaches A^*.
3) *Hours–days:* lesion processing carries X toward $X^* = \Xi$, macroscopic performance integrates $S(R, A)$ and $L(X)$.
4) *Generations:* selection acts on induced variants, P_{mut} becomes a breeding-relevant quantity.

Each boundary in this hierarchy suggests an experimental lever: shortening exposures to avoid A induction will raise Ξ at fixed D; allowing recovery intervals reduces X and lowers $\Lambda(D)$, manipulating moisture or oxygen shifts σ_R, η and hence R^*.

Table 2: Summary of principal parameters used in the kinetic model and unified dose–effect model. Symbols correspond to the kinetic model and dose–response formulation introduced above.

Symbol	Meaning	Biological interpretation	Typical units or range
κ	Dose-to-radical conversion factor	Efficiency of radiochemical energy transfer to ROS production	$\mathrm{mol\,L^{-1}\,Gy^{-1}\,s^{-1}}$
σ_R	Linear scavenging rate	Basal ROS removal by antioxidants and diffusion	$\mathrm{s^{-1}}$
η	Quadratic recombination rate	Radical–radical termination efficiency	$\mathrm{L\,mol^{-1}\,s^{-1}}$
$\alpha_0,\ \alpha_1$	Basal / inducible antioxidant synthesis rates	Constitutive vs. ROS-induced enzyme expression	arbitrary units $\mathrm{s^{-1}}$
σ_A	Antioxidant turnover rate	Degradation or inactivation of antioxidant capacity	$\mathrm{s^{-1}}$
λ	Lesion formation coefficient	Probability of DNA lesion per radical load	lesions $\mathrm{mol^{-1}}$
ρ	Repair throughput coefficient	Efficiency of A-dependent lesion repair	arbitrary units $\mathrm{s^{-1}}$
μ	Baseline repair rate	A-independent repair and excision mechanisms	$\mathrm{s^{-1}}$
Ξ	Repair challenge number	Ratio of lesion inflow to effective repair throughput; regime index	dimensionless
$D_f,\ p$	Fidelity parameters	Dose at half repair fidelity; steepness of fidelity loss	Gy, dimensionless
c, d, f, e, b, q, r	Dose–effect coefficients	Parameters controlling low-dose slope, curvature, and damage-dominated decline	fitted from $E(D)$ data

3. Results

We analyze the composite model introduced in (10),

$$E(D) = \mathcal{H}(D) - \mathcal{L}(D), \qquad \mathcal{H}(D) = c + \frac{(d-c) + fD}{1 + (D/e)^b}, \qquad \mathcal{L}(D) = q\,D^r,$$

under the standing constraints $d > c$, $f > 0$, $e > 0$, $b > 1$, $q > 0$, $r > 1$. The aim is to record the shape properties used later (initial slope, curvature near the origin, existence and uniqueness of an interior maximizer, asymptotics), express them in a nondimensional form, and indicate how the kinetic index Ξ in (9) annotates the dose axis.

For conciseness write $g(D) = (d-c) + fD$ and $h(D) = 1 + (D/e)^b$, so $\mathcal{H} = c + g/h$. Differentiating,

$$\mathcal{H}'(D) = \frac{g'(D)\,h(D) - g(D)\,h'(D)}{h(D)^2} = \frac{f\,[1 + (D/e)^b] - \left[(d-c) + fD\right]\frac{b}{e^b}D^{\,b-1}}{\left[1 + (D/e)^b\right]^2}. \tag{14}$$

At $D = 0$ and for $b > 1$ one has $h'(0) = 0$, hence $\mathcal{H}'(0) = f > 0$. The second derivative at the origin depends on b; in particular:

$$\mathcal{H}''(0) = \begin{cases} -\dfrac{2(d-c)}{e^2} & \text{if } b = 2, \\ 0 & \text{if } b > 2, \end{cases}$$

while for $1 < b < 2$ the second derivative diverges at 0 but the finite one-sided slope $\mathcal{H}'(0) = f$ still holds. Thus the hormetic channel starts increasing and bends down shortly after the origin for all $b > 1$. For large dose,

$$\mathcal{H}(D) = c + \frac{(d-c) + fD}{1 + (D/e)^b} \sim c + f\, e^{\,b} D^{\,1-b} \quad (D \to \infty),$$

so $\mathcal{H}(D) \downarrow c$ with vanishing negative slope. The penalty satisfies $\mathcal{L}'(D) = qr\, D^{r-1}$ and $\mathcal{L}''(D) = qr(r-1)D^{r-2} \geq 0$. Therefore,

$$E'(0) = \mathcal{H}'(0) - \mathcal{L}'(0) = f > 0, \qquad \lim_{D\to\infty} E'(D) = -\infty,$$

and E must possess at least one interior stationary point.

It is convenient to normalize variables. Let $x = D/e$ and $\tilde{E} = (E - c)/(d - c)$. With $\phi = \frac{fe}{d-c} > 0$ and $\tilde{q} = \frac{qe^r}{d-c} > 0$,

$$\tilde{E}(x) = \frac{1 + \phi x}{1 + x^b} - \tilde{q}\, x^r, \qquad b > 1,\ r > 1. \tag{15}$$

Then $\tilde{E}'(0) = \phi > 0$ and $\lim_{x\to\infty} \tilde{E}'(x) = -\infty$, ensuring an interior maximizer $x^* > 0$. As $\tilde{q} \downarrow 0$, the maximizer x^* converges to the unique maximizer of $(1 + \phi x)/(1 + x^b)$, and, for fixed b, r, x^* increases with ϕ (stronger low-dose gain) and decreases with $\tilde{q}$ (stronger penalty). These monotone movements will be used below when discussing interventions.

We adopt the regime index already defined,

$$\Xi(u) = \frac{\lambda\, R^*(u)}{\rho\, A^*(u) + \mu}, \qquad A^*(u) = \frac{\alpha_0 + \alpha_1 R^*(u)}{\sigma_A},$$

which is continuous and strictly increasing in the physical drive u, with $\Xi(0) = 0$. If inducible antioxidants operate ($\alpha_1 > 0$), Ξ admits the finite ceiling

$$\Xi_\infty = \lim_{u\to\infty} \Xi(u) = \frac{\lambda\, \sigma_A}{\rho\, \alpha_1}. \tag{16}$$

Under constant-rate protocols ($u = D/T$) one obtains a monotone map $D \mapsto \Xi(D)$ and, by inversion, operational markers $D(\Xi_-)$ and $D(\Xi_+)$ locating adaptive, mutagenic and sterilizing zones along the dose axis. This gives a direct way to annotate empirical curves with mechanistic content.

Existence and operational uniqueness of a performance maximum: Let $E(D)$ be as in (10), with $f > 0$, $b > 1$, $q > 0$ and $r > 1$. Then $E'(0) = f > 0$ and $E'(D) \to -\infty$ as $D \to \infty$, so at least one interior maximizer exists. In the parameter ranges of interest, where the adaptive component is unimodal and the damage penalty is monotone and convex, this maximizer is operationally unique. Under these conditions E increases before D^* and decreases after D^*. Moreover D^* depends continuously on $(\phi, \tilde{q})$ in (15), increasing with ϕ and decreasing with $\tilde{q}$.

$E'(0) = f > 0$ and $\lim_{D\to\infty} E'(D) = -\infty$ guarantee at least one interior zero of E'. The derivative E' is strictly decreasing in the right tail because $\mathcal{L}'$ is increasing and $\mathcal{H}'$ tends to 0^-. At low dose, the numerator of (14) is strictly decreasing after a small neighborhood of zero, ensuring E' crosses zero once. Continuity and strict monotonicity on either side of D^* yield unimodality. Monotone dependence on $(\phi, \tilde{q})$ follows from implicit differentiation of $E'(D^*; \phi, \tilde{q}) = 0$ and the signs $\partial_\phi E' > 0$, $\partial_{\tilde{q}} E' < 0$.

Two practical approximations for D^* are adequate for design. In a low-penalty regime (small $\tilde{q}$), the maximizer lies near $D^*_{\mathcal{H}} = e\, \psi(b, \phi)$, the unique solution to $\mathcal{H}'(D) = 0$, with a first-order Newton correction on E'. Conversely, when the decline is strong, a simple balance yields

$$qrD^{r-1} \approx \frac{f}{\left[1 + (D/e)^b\right]^2}, \tag{17}$$

whose unique positive root provides D^*.

We also record the minimal well-posedness facts for the kinetic backbone (4)–(6). For any bounded measurable $u(t) \geq 0$ and nonnegative initial data, the system admits a unique global nonnegative solution; $R(t)$ and $A(t)$ remain bounded for bounded u, and $X(t)$ is bounded whenever $\inf_t\{\rho A(t) + \mu\} > 0$. At constant u, $R \to R^*(u)$ and $A \to A^*(u)$ monotonically; substituting into $\dot{X} = \lambda R - (\rho A + \mu)X$ gives $\dot{X} = (\rho A^* + \mu)(\Xi - X)$ so that $X(t) \to X^*(u) = \Xi(u)$ exponentially. Thus Ξ equals the steady normalized lesion burden and monotonically orders regimes.

Finally, we connect repair fidelity to mutation probability. Let $F(D) = \left[1 + (D/D_f)^p\right]^{-1}$, with $D_f > 0$, $p > 0$, and define

$$P_{\mathrm{mut}}(D) = 1 - \exp\{-\lambda\, D\,[1 - F(D)]\}. \tag{18}$$

Then P_{mut} increases smoothly from 0 to 1, with the low-dose expansion

$$P_{\mathrm{mut}}(D) \sim \lambda\, \frac{D^{p+1}}{D_f^{\,p}} \qquad (D \ll D_f),$$

and $P_{\mathrm{mut}}(D) \to 1 - e^{-\lambda D}$ for $D \gg D_f$. Because $F(D)$ declines as Ξ approaches unity, D_f approximates the position where adaptive control fails ($\Xi \approx 1$). For fixed cumulative dose D, lower rate u permits antioxidant induction ($\alpha_1 > 0$), reduces Ξ, and lowers P_{mut} (dose-rate sparing).

4. Discussion

We now interpret the composite response $E(D)$ and the fidelity-driven $P_{\mathrm{mut}}(D)$ against empirical regularities and practical aims. The posture is conservative: we do not claim new effects, we propose a single control structure that rationalizes familiar patterns and clarifies levers for design.

A useful picture is a single curve $E(D)$ annotated by Ξ-contours along the abscissa. On the left, where $\Xi \ll 1$, $F(D) \approx 1$ and E rises with dose, mutation is negligible. Around the interior maximum, Ξ approaches unity, fidelity declines, and the system enters a narrow band where performance remains acceptable but misrepair becomes nontrivial. Farther right, $\Xi \gg 1$, $F(D) \to 0$, and the penalty dominates. There is, then, a healthy zone of instability: it denotes the region where modest infidelity is tolerated without catastrophic loss of function. Its position and width are not universal constants, they shift with genotype and environment through α_1 (inducibility), ρ (repair throughput), κ, σ_R, η (radiochemical sinks) and σ_A (turnover).

The model offers direct, monotone predictions. Interventions that increase inducibility or repair (larger α_1 or ρ) reduce Ξ at a given u, effectively increasing the characteristic scale e in (10), pushing D^* to the right and widening the useful band. Higher instantaneous u at fixed cumulative D increases Ξ (less time for induction), shrinking e and steepening the decline. Greater moisture or oxygen typically increases κ and reduces σ_R, accelerating Ξ's growth with u and narrowing the window. These signs match common physiological observations.

The fidelity link (18) ties genetic outcomes to the same structure. Three consequences are immediate. First, low-dose scaling: for $D \ll D_f$, P_{mut} scales as D^{p+1}; the exponent > 1 explains why mutagenesis is so hard to detect near the hormetic peak. Second, dose-rate sparing: for equal D, lower u reduces Ξ and therefore reduces $\Lambda(D) = \lambda D[1 - F(D)]$, provided $\alpha_1 > 0$. Third, co-movement: interventions that right-shift $E(D)$'s maximum also right-shift the onset of appreciable P_{mut}, because both are governed by the approach of Ξ to unity.

For practice, the framework suggests a physiology-first workflow. One may fit (10) to an easily measured endpoint (hypocotil emergence, early biomass) and extract D^*, the net peak gain $H_{\max} = E(D^*) - c$ and a tolerance window $W(\delta) = \{D :\ E(D) \geq c + (1 - \delta)H_{\max}\}$. If even sparse fidelity proxies are available (three doses spanning low, near-peak, high), fitting $F(D) = 1/(1 + (D/D_f)^p)$ stabilizes the mapping from e to D_f and helps bound q, r. Absent such data, e can be used as a surrogate for the dose at which $\Xi \approx 1$ in comparative studies. Dose placement then follows the stated aim: to enhance vigor without genetic change, operate well within the left half of $W(0.1)$ and prefer lower rate, to discover mutations with manageable viability loss, operate just beyond D^* while enforcing a viability floor, to sterilize for phytosanitary purposes, operate past $D(\Xi_+)$ with a margin.

The proposed envelope nests familiar limiting descriptions. When the penalty is negligible ($q \to 0$), $E \to \mathcal{H}$ and the curve reduces to a classical hormetic shape. When the adaptive gain is negligible for a given endpoint, $E \approx -\mathcal{L}$ and one recovers monotone decreasing behavior.

As a simple practical example, an experimenter interested in seed vigor could expose several seed lots to a small dose series, fit (10) to germination percentage or early biomass, and define a useful window as the set of doses that preserve a fixed fraction of the fitted maximum response. If a treatment that increases antioxidant inducibility raises α_1, the model predicts a lower Ξ at the same dose rate, a rightward shift of the useful window, and a delayed onset of the fidelity penalty. Conversely, if the same cumulative dose is delivered at a higher dose rate, the model predicts less time for inducible protection and therefore a narrower safe window.

The present formulation is intentionally minimal and should be read as a theoretical organizing scaffold rather than as a validated predictive model for a particular crop. Its parameters must be estimated separately for each biological material, endpoint and irradiation protocol. Empirical validation would require dose–response data collected together with at least one oxidative-stress marker and one repair or fidelity proxy. Accordingly, the main contribution of the model is not the introduction of new experimental data, but the explicit statement of testable relationships among dose rate, redox compensation, repair challenge and macroscopic outcome.

We close with brief remarks on scope and testing. The kinetic balances are lumped and deliberately minimal. Many details (species of ROS, organelle-specific signaling, cross-talk) are compressed into aggregate parameters, our claim is only that the control structure is visible and manipulable. The most informative experiments for parameterizing this backbone are those that combine multiple doses and at least two dose-rates, include antioxidant activity assays to constrain (α_1, σ_A) and collect a simple fidelity proxy to constrain (D_f, p). Even partial adherence to these elements makes shifts in $\phi, b, \tilde{q}$ interpretable on kinetic grounds. Such detailed experiments are, alas, rare.

5. Conclusion

This work sought to place physiological stimulation, mutagenesis and sterilization on a single, continuous radiobiological axis governed by redox dynamics and repair capacity. To that end, we developed a minimal kinetic scaffold that links reactive oxygen species, inducible antioxidant defenses and lesion processing, and we collected their balance into a nondimensional *repair challenge number* Ξ. On this basis, we proposed a unified dose–effect model $E(D)$ that reproduces the familiar hormetic rise at low doses and the damage-dominated decline at higher doses, with an interior maximum that is operationally unique under mild unimodality assumptions.

The practical value of this formulation is its economy and interpretability. Annotating the dose axis with Ξ, the same mathematics that explains performance gains also predicts when repair fidelity begins to erode. A simple fidelity function $F(D)$ connects the position of the performance peak to the onset of misrepair, clarifying why low-dose stimulation can coexist with negligible mutational yield and why dose-rate, moisture and genotype shift the "useful window" in consistent directions. We hope this common language aids experimental design (e.g., dose and rate selection, priming strategies, ontologies), improves comparability across studies, and encourages joint reporting of performance and fidelity proxies.

References

[1] Alves, L.F.M. and Arthur, V., Ionizing radiation in agriculture: physical, biological and ontological approaches, Seven Editora, pp. 36–74, 2025.

[2] Alves, L.F.M. and Arthur, V., Biomathematical approach to hormetic dose–response and varietal radiosensitivity in nicotiana tabacum L, TSF Journal of Biology, 3(2), pp. 26–51, 2025.

[3] Geng, X., Zhang, Y., Wang, L. and Yang, X., Pretreatment with high-dose gamma irradiation on seeds enhances the tolerance of sweet osmanthus seedlings to salinity stress, Forests, 10(5), p. 406, 2019.

[4] International Atomic Energy Agency, Mutant variety database for climate-smart crops enhanced with new tools and features, IAEA News Center, 2026. https://www.iaea.org/newscenter/news/mutant-variety-database-for-climate-smart-crops-enhanced-with-new-tools-and-features, Accessed on June 19, 2026.

[5] Kotsyubinskaya, O.A., Bondarenko, E.V., Kazydub, N.G., and Blinova, Y.A., Effect of gamma irradiation of seeds on the development of Phaseolus vulgaris L. plants, Vegetable Crops of Russia, 1, pp. 37–44, 2025.

[6] Mussi, C., Nakayama, H. and Oviedo de Cristaldo, R., Variabilidad fenotípica en poblaciones M1 de sésamo (Sesamum indicum L.) irradiado con rayos gamma, Cultivos Tropicales, 37, pp. 74–80, 2016.

[7] Samudio-Oggero, A., Romero, G.A.R., Vergara, W.D.R., Alvarenga, O.J.V., Núñez, J.V.B., Tórres, B.O., Romero, P.C.C. and González, M.C.C., Determination of the method of induction of mutations by gamma radiation in soybeans (Glycine max L. Merrill) for tolerance to carbonic rot produced by the fungus Macrophomina phaseolina (Tassi Goid.), MethodsX, 14, p. 103251, 2025.

[8] Savov, P.G., Radiation mutagenesis in wheat, Agricole Publishing Academy, New Delhi, 1989.

[9] Spencer-Lopes, M.M., Forster, B.P., and Jankuloski, L., Manual on mutation breeding (3rd ed.), Food and Agriculture Organization of the United Nations and International Atomic Energy Agency, Rome/Vienna, 2018.

[10] Villegas, D., Sepúlveda, C. and Ly, D., Use of low-dose gamma radiation to promote the germination and early development in seeds, In Seed Biology-New Advances, IntechOpen, 2023.

[11] Vose, P.B., Introduction to nuclear techniques in agronomy and plant biology, Pergamon Press, Oxford, 1980.